Transceiver inphase/quadrature-imbalance, ellipse fitting, and the universal software radio peripheral

Cristian R. Rojas, Per Zetterberg, and Peter Händel, *Senior Member, IEEE*

***Abstract*—In this paper we introduce a method for IQ imbalance parameter estimation based on ellipse fitting. The performance of the method is analytically derived. In particular, it is shown that the method exhibits a small bias (which can be negligible under some standard practical conditions) and a variance slightly above the Cramér-Rao bound. The method is then applied to measurements from a contemporary BiCMOS transceiver which is used on one of the most popular daughterboards of the universal software peripheral (USRP). In our measurements the phase skew varies up to five degrees with the base-band frequency, while the amplitude imbalance varies between $0-0.3$ dB over carrier frequencies and across hardware units. The time variation however is only 0.004 dB in amplitude and 0.06 degrees in phase. This indicates that the units could either be calibrated on-line when there is no transmission (in a two antenna MIMO system one antenna could transmit a calibration signal to the other), or they could be calibrated during production, in which a case a table with different carrier and base-band frequencies would be needed. However, there is no need to estimate the parameters on every burst.**

***Index Terms*—inphase/quadrature (IQ) imbalance, Cramér-Rao bounds, ellipse fitting, universal software radio peripheral USRP.**

I. Introduction

TIME-EFFICIENT test methods are a requirement for effective large-volume production tests of electronic devices. Radio transceivers are a pervasive component in consumer and industrial electronics produced in immense volumes, for example mobile phones, wireless local area network routers, remote controls, and so on.

This work considers a fully digital and software implementable time-efficient method for determination of the inphase/quadrature (IQ) imbalance of contemporary direct-conversion radio frequency transceivers based only on the digital baseband output. The method is derived from the practice of measuring the imbalance by manual reading of elliptic *Lissajous* plots presented by a dual beam cathode ray tube (CRT) oscilloscope [1]. Considering a receiver, a perfectly balanced one should display a circle centered on the CRT-screen, whereas practical receivers display an ellipse because of the gain imbalance between the I and Q channels, and the quadrature skew or phase offset. The center of the ellipse is offset from the center of the display due to the leakage from the local oscillator (LO).

The research leading to these results has received funding from the European Research Council under the European Community's Seventh Framework Programme (FP7/2007-2013) / ERC grant agreement no. 228044.

The authors are with the ACCESS Linnaeus Center, Royal Institute of Technology, Stockholm, Sweden. Emails: cristian.rojas@ee.kth.se, perz@s3.kth.se and ph@kth.se.

Fitting the parameters of an ellipse to noisy sampled data is a problem of great interest in several communities, including two dimensional image processing [2], medical imaging [3], and computer vision [4], [5], [6], [7], [8]. A seminal contribution to the algorithmic development of robust ellipse fitters was Fitzgibbon's method [2]. The ingenuity of the method in [2] is the relaxation of the elliptic constraint imposed on the solution, leading to a problem with a closed form solution. From an instrumentation and measurement point of view, the method in [2] is a way to replace a manual reading of an elliptic *Lissajous* plot [9], by automatic digital signal processing of A/D converter samples. Within the instrumentation and measurement community, the fitting of an ellipse makes sense, see e.g. the work on estimation of particle size and velocity in laser anemometry [10], [11], and impedance determination [12], [13], [14], [15]. Some numerical characterizations of the ellipse fitting in [2] to the problem of impedance characterization were presented in [12], [13] highlighting some systematic or bias errors, especially for scenarios with low signal-to-noise ratios. One of the contributions of this work is a detailed analysis of this systematic error.

For scenarios characterized by an additive noise model, a detailed theoretic performance assessment was performed in [16]. In [16], under a Gaussian assumption, the ultimate performance of any unbiased estimator was addressed by the Cramér-Rao lower bound [17]. In addition, the performance of nonlinear least squares estimation of the sought parameters (for example, the method in [18] which is a generalization of the IEEE standardized tone fit algorithm to dual channels, [19]) was investigated. Nonlinear least-squares estimation to characterize IQ-imbalance of direct-conversion receivers was considered in [20], revealing not only the excellent performance of the nonlinear least-squares method in general, but also its outlier performance under stressed situations aiming at reducing the testing time.

The purpose of this paper is threefold. First, the performance of the popular method in [2] is analyzed in detail in an attempt to characterize the earlier observed systematic error, as well as the accuracy of the same method. In addition, the performance of the method is compared with objective bounds on the achievable performance [16], quantifying the loss in performance compared with statistically efficient methods – the price paid for the low numerical complexity of the employed method.

Secondly, the ellipse fitting approach is used to characterize the IQ imbalance of a contemporary BiCMOS radio frequency transceiver, namely, the MAXIM 2829 (www.maxim-ic.com/datasheet/index.mvp/id/4532/t/al). The setup is designed to

allow the characterization of the transmitter as well as the receiver. We investigate the IQ imbalance as a function of base-band frequency, carrier frequency, time and across five different hardware units. We find that the IQ imbalance is clearly varying with all the above parameters except time. This indicates that the units could be calibrated during production in which case a table with different carrier frequencies would be needed. Another alternative would be to do calibration when the unit is idle.

Contemporary and future wireless communication systems put high demands on accurate and time-efficient test methods for production and product validation, especially for multiple input multiple output (MIMO) systems, where each branch is equipped with its own transceiver. A suitable method should provide estimates with low bias and variance while at the same time require a limited amount of computations. As indicated in [12], ellipse fitting is computationally less demanding than brute-force nonlinear least-squares methods.

Thirdly, the MAXIM 2829 is used in one of the most popular daughterboards of the universal software radio peripheral (USRP). The USRP has entered the research community as a versatile radio platform for education, development and research [21], with applications aiming at navigation [22], cognitive radio [23], and software defined radio [24]. Thus the results obtained herein have an interest of their own, owing to the widespread use of the USRP.

The paper is organized as follows. In Sec. II, the problem is formulated, and the state-of-the art is reviewed. The performance analysis is performed in Sec. IV. The evaluation on a set of MAX2829 is presented in VI. Finally, the conclusions are drawn in Sec. VII.

II. Problem Set-up and State-of-the Art

In the subsequent paragraphs, the measurements are introduced, different parameterizations of the signal model are discussed, and benchmarks bounds and methods are shortly reviewed.

A. Measurements

Consider the dual-channel measurements

$$y_1(1),\ldots,y_1(N),\, y_2(1),\ldots,y_2(N). \tag{1}$$

where the subscript denotes the channel number, and n denotes the running time index, $n=1,\ldots,N$. Thus, in total there are $2N$ recorded samples, which form the basis for extracting the parameters of interest. These parameters depend on the application in mind, as outlined in the sequel.

B. A Parametric Model

A parametric model of the measurements is considered, where the unknown parameters are gathered in the parameter vector θ, that is

$$y_1(n;\theta) = s_1(n;\theta) + v_1(n) \tag{2}$$

and

$$y_2(n;\theta) = s_2(n;\theta) + v_2(n). \tag{3}$$

In (2)-(3), $s_k(n;\theta)$ (for $k=1,2$) denotes the undistorted output, and $v_k(n)$ a noise term, including additive thermal noise, model imperfections, quantization, harmonic distortion, and so on. The source signal in the first channel is modeled by

$$s_1(n;\theta) = A_1\cos(\omega_0\, n) + B_1\sin(\omega_0\, n) + C_1 \tag{4}$$

where A_1 and B_1 are the amplitudes of the in-phase and quadrature components and C_1 is the DC-level. The quantity ω_0 denotes the normalized angular (base-band) frequency, that is $\omega_0 = 2\pi F/F_S$, where F is the absolute frequency in Hertz and F_S the sampling frequency. In a similar vein, the parametric model for the second channel reads

$$s_2(n;\theta) = A_2\cos(\omega_0\, n) + B_2\sin(\omega_0\, n) + C_2. \tag{5}$$

As noted in (4) and (5), the sinewave frequency ω_0 is common to both channels. Here, the parameter vector θ with the seven unknown parameters is defined as

$$\theta := [A_1\ B_1\ C_1\ \omega_0\ C_2\ B_2\ A_2]^T$$

where ^{T} denotes the transpose operation.

C. Alternative parameterizations and their relevance

In many applications (as outlined later on), the interest lies in the estimations of the A_k, B_k and C_k and transformations thereof, and thus ω_0 may be considered as a nuisance parameter. An alternative parametrization includes the amplitude-phase model

$$y_1(n;\theta) = \alpha_1\cos(\omega_0\, n) + C_1 + v_1(n) \tag{6}$$

$$y_2(n;\theta) = \alpha_2\cos(\omega_0\, n + \phi_\Delta) + C_2 + v_2(n) \tag{7}$$

with $\alpha_k = \sqrt{A_k^2 + B_k^2}$. In (6), we have fixed the initial phase of the first channel, and introduced the phase difference ϕ_Δ in (7). For later reference, let us the parameter vector

$$\vartheta := [\alpha_1\ \alpha_2\ \phi_\Delta\ C_1\ C_2]^T. \tag{8}$$

Other parameterizations include relative amplitude differences $\alpha_\Delta := \alpha_1 - \alpha_2$ and quotients $\alpha_\Pi := \alpha_2/\alpha_1$. In particular: *i)* for phase doppler anemometry the parameters of interest are the angular frequency ω_0, which is proportional to the velocity, and the phase difference ϕ_Δ that determines the particle size [10], [11], *ii)* for impedance measurements the parameters of interest are the phase difference ϕ_Δ and amplitude quotient α_Π [12], [13], and *iii)* for mixer imbalance measurements [20], [25], the parameters of interest are:

- The *gain imbalance*

$$G := \alpha_\Pi = \frac{\alpha_2}{\alpha_1}, \tag{9}$$

- The *quadrature skew*

$$Q := \frac{\pi}{2} - \phi_\Delta,$$

- The *LO leakage*

$$L := 2\frac{C_1^2 + C_2^2}{\alpha_1^2 + \alpha_2^2}. \tag{10}$$

One may note that the model in (6)-(7) is slightly less general than (2)-(5) because of the alignment of the initial phases. For the problem at hand, however, it imposes no restrictions.

D. Benchmarks: ML, NLS and CRB

Let the error terms in (2)–(3) be modeled as jointly independent zero mean Gaussian white noises with variances σ_1^2 and σ_2^2, respectively. In the Gaussian scenario, the method of maximum likelihood (ML) is given by the minimizer $\hat{\theta}_{\text{ML}}$ of the least-squares criterion, which is [11]

$$\hat{\theta}_{\text{ML}} = \arg \min_{\theta,\, \sigma_1^2,\, \sigma_2^2} \sum_{k=1}^{2} \frac{1}{\sigma_k^2} \sum_{n=1}^{N} \left(y_k(n) - s_k(n;\theta)\right)^2 .$$

Following the methodology in [11], an estimator may be derived. The performance in terms of error variance of such an estimator is expected (at least as $N \to \infty$) to coincide with the Cramér-Rao bound (CRB) on error performance [17]. However, the ML estimator depends on the unknown noise variances. In [16], the nonlinear least-squares estimator $\hat{\theta}_{\text{NLS}}$ was investigated:

$$\hat{\theta}_{\text{NLS}} = \arg \min_{\theta} \sum_{k=1}^{2} \sum_{n=1}^{N} \left(y_k(n) - s_k(n;\theta)\right)^2 .$$

The study in [16] revealed that the estimates were obtained with an accuracy that basically coincides with the CRB for a wide span of channel signal-to-noise ratios. It is obvious that the numerical complexity obtaining the latter estimate is lower than for the ML, because of the independence of the noise variances. In summary, the nonlinear-least squares estimate $\hat{\theta}_{\text{NLS}}$ is favorable over $\hat{\theta}_{\text{ML}}$. One may note that $\hat{\theta}_{\text{NLS}}$ is studied in some detail in [18], where in particular an efficient algorithm for its implementation is proposed. One may note the similarities between the seven-parameter fit algorithm presented in [18] and the the IEEE standardized four-parameter fit for the single channel case [19]. The excellent performance of the algorithm in [18] is also demonstrated in [16].

The CRB is an objective bound on the achievable estimation error variance of any method [17]. In practice, it is feasible to derive the bound for unbiased estimators under the Gaussian assumption, as shown in [19]. This result was further refined in [26] following the derivations in the classical paper [27]. The generalization of the CRB to the seven-parameter model (2)-(5) was derived in [16]. Transformed values for G, Q and L according to (9)–(10) are found in [20]. For easy reference, the key results on the CRB are presented in Table I. Here, the signal-to-noise ratio (SNR) per measurement channel is defined as (for $k = 1, 2$)

$$\text{SNR}_k := \frac{A_k^2 + B_k^2}{2\sigma_k^2} = \frac{\alpha_k^2}{2\sigma_k^2}. \tag{11}$$

In our work, the CRB results in Table I serve as baseline for the employed ellipse fitting algorithm for the problem at hand. It is worth remarking that similar CRB results have been derived in [28], [29], [30] for curve and surface estimation, where the time information associated with the measurements is not available (i.e., the frequency ω_0 becomes a nuisance parameter).

TABLE I: CRB for different transformations of the parameters in the two-channel sinewave model (for $k = 1, 2$) [16], [20].

parameter φ	CRB(φ)
in-phase component A_k	$\frac{1}{N}\left(2\,\sigma_k^2 + \frac{3\,B_k^2}{\text{SNR}_1+\text{SNR}_2}\right)$
quadrature component B_k	$\frac{1}{N}\left(2\,\sigma_k^2 + \frac{3\,A_k^2}{\text{SNR}_1+\text{SNR}_2}\right)$
DC-level C_k	$\frac{\sigma_k^2}{N}$
angular frequency ω_0	$\frac{12}{N^3(\text{SNR}_1+\text{SNR}_2)}$
amplitude α_k	$\frac{2\,\sigma_k^2}{N}$
initial phase ϕ_k	$\frac{1}{N\,\text{SNR}_k}\left(1 + \frac{3\,\text{SNR}_k}{\text{SNR}_1+\text{SNR}_2}\right)$
amplitude difference α_Δ	$\frac{2\,(\sigma_1^2+\sigma_2^2)}{N}$
phase difference ϕ_Δ (also Q)	$\frac{\text{SNR}_1+\text{SNR}_2}{N\,\text{SNR}_1\,\text{SNR}_2}$
amplitude quotient α_Π (also G)	$\frac{\alpha_\Pi^2}{N}\left(\frac{1}{\text{SNR}_1} + \frac{1}{\text{SNR}_2}\right)$
LO leakage L ($\text{SNR}_1 = \text{SNR}_2$)	$\frac{2L(1+L)}{N\text{SNR}}$

III. Ellipse fitting

In this section we revisit the ellipse fitting algorithm of [2]. To this end, we first introduce some definitions and assumptions. Consider two sinusoidal signals given by (6)-(7), where $\alpha_1 \in \mathbb{R}_0^+$, $\alpha_2 \in \mathbb{R}_0^+$, $\phi_\Delta \in (-\pi, \pi] \setminus \{0\}$, $C_1 \in \mathbb{R}$ and $C_2 \in \mathbb{R}$ are unknown constants to be estimated, and $\omega_0 \in \mathbb{R}^+$ is an unknown nuisance parameter. The sequences $\{v_1(n)\}_{n\in\mathbb{N}}$ and $\{v_2(n)\}_{n\in\mathbb{N}}$ are jointly independent Gaussian white noise signals of zero mean and variances σ_1^2 and σ_2^2, respectively.

The ellipse fitting algorithm is based on the observation that the noiseless points $\{(y_1(n) - v_1(n), y_2(n) - v_2(n))\}_{n\in\mathbb{N}}$ belong to an ellipse [2].

A. Ellipse parameters

From (6)-(7) we have that

$$\left(\frac{y_1 - v_1 - C_1}{\alpha_1}\right)^2 + \left(\frac{[y_1 - v_1 - C_1]\cos(\phi_\Delta)}{\alpha_1 \sin(\phi_\Delta)} - \frac{y_2 - v_2 - C_2}{\alpha_2 \sin(\phi_\Delta)}\right)^2 = 1$$

where we have dropped the argument n for simplicity. This can be can be further simplified to yield a quadratic form in $x := y_1 - v_1$ and $y := y_2 - v_2$ of the form

$$ax^2 + bxy + cy^2 + dx + ey + f = 0 \tag{12}$$

where

$$\begin{aligned}
a &:= \alpha_2^2 \\
b &:= -2\alpha_1\alpha_2\cos(\phi_\Delta) \\
c &:= \alpha_1^2 \\
d &:= 2\alpha_1\alpha_2\cos(\phi_\Delta)C_2 - 2\alpha_2^2 C_1 \\
e &:= 2\alpha_1\alpha_2\cos(\phi_\Delta)C_1 - 2\alpha_1^2 C_2 \\
f &:= \alpha_2^2 C_1^2 + \alpha_1^2 C_2^2 - 2\alpha_1\alpha_2\cos(\phi_\Delta)C_1C_2 - \alpha_1^2\alpha_2^2\sin^2(\phi_\Delta).
\end{aligned}$$

This set of equations defines a mapping from the parameters in ϑ of (6)-(7) to the coefficients

$$\eta := [a\ b\ c\ d\ e\ f]^T \tag{13}$$

of the quadratic form (12). Notice that, since (12) defines an ellipse, it holds that $f \neq 0$ and $f(b^2 - 4ac) > 0$.

The mapping (12) is not invertible, since (12) is invariant with respect to multiplication by a nonzero constant. To solve this issue, we can scale (12) so that $4ac - b^2 = 1$ (which imposes $f < 0$). Under such condition, we arrive at the inverse mapping:

$$\begin{aligned} \alpha_1 &= \sqrt{kc} \\ \alpha_2 &= \sqrt{ka} \\ \cos(\phi_\Delta) &= -\frac{b}{2\sqrt{ac}} \\ C_1 &= be - 2cd \\ C_2 &= bd - 2ae; \quad k = 4(cd^2 - bde + ae^2 - f). \end{aligned} \tag{14}$$

The relations between the six parameters gathered in η in (13) and five ones gathered in ϑ in (8) are given by

$$\begin{aligned} a &= \frac{\alpha_2}{2\alpha_1|\sin(\phi_\Delta)|} \\ b &= -\frac{\cos(\phi_\Delta)}{|\sin(\phi_\Delta)|} \\ c &= \frac{\alpha_1}{2\alpha_2|\sin(\phi_\Delta)|} \\ d &= \frac{\cos(\phi_\Delta)}{|\sin(\phi_\Delta)|}C_2 - \frac{\alpha_2}{\alpha_1|\sin(\phi_\Delta)|}C_1 \\ e &= \frac{\cos(\phi_\Delta)}{|\sin(\phi_\Delta)|}C_1 - \frac{\alpha_1}{\alpha_2|\sin(\phi_\Delta)|}C_2 \\ f &= \frac{\alpha_2}{2\alpha_1|\sin(\phi_\Delta)|}C_1^2 + \frac{\alpha_1}{2\alpha_2|\sin(\phi_\Delta)|}C_2^2 \\ &\quad - \frac{\cos(\phi_\Delta)}{|\sin(\phi_\Delta)|}C_1C_2 - \frac{\alpha_1\alpha_2}{2}|\sin(\phi_\Delta)|. \end{aligned} \tag{15}$$

B. Algorithm

We now have the problem of how to fit an ellipse to the data (1). For easy reference, the method in [2] is shortly reviewed below. Form the matrices

$$\mathbf{D} := \begin{bmatrix} y_1^2(1) & y_1(1)\,y_2(1) & y_2^2(1) & y_1(1) & y_2(1) & 1 \\ \vdots & & \vdots & \vdots & \vdots & \vdots \\ y_1^2(N) & y_1(N)\,y_2(N) & y_2^2(N) & y_1(N) & y_2(N) & 1 \end{bmatrix}$$

$$\mathbf{C} := \begin{bmatrix} 0 & 0 & 2 & 0 & 0 & 0 \\ 0 & -1 & 0 & 0 & 0 & 0 \\ 2 & 0 & 0 & 0 & 0 & 0 \\ 0 & 0 & 0 & 0 & 0 & 0 \\ 0 & 0 & 0 & 0 & 0 & 0 \\ 0 & 0 & 0 & 0 & 0 & 0 \end{bmatrix} \tag{16}$$

and the parameter vector η in (13). Then, estimate η as

$$\hat{\eta} = \arg\min_{\eta} \eta^T\,\mathbf{D}^T\mathbf{D}\,\eta \quad \text{s.t.} \quad \eta^T\,\mathbf{C}\,\eta = 1. \tag{17}$$

The solution of (17) can be obtained by computing the generalized eigenvectors of $(\mathbf{D}^T\mathbf{D}, \mathbf{C})$, i.e., by solving the equation $\mathbf{D}^T\mathbf{D}x = \lambda\mathbf{C}x$ for λ and x, subject to the constraint $x^T\,\mathbf{C}\,x = 1$. As it was shown in [2], there is a unique positive solution for λ, and $\hat{\eta}$ corresponds to the solution x associated with such $\lambda > 0$. Finally, the estimate $\hat{\vartheta}$ (c.f. (8)) can be computed from $\hat{\eta}$ using the relations (14).

IV. Performance Analysis

We are first interested in the accuracy of $\hat{\vartheta}$ in (8) when ellipse fitting is applied. The performance of the other parameters (c.f. Table I) are then obtained by proper transformations.

In order to study the performance of the ellipse fitting algorithm, we proceed in three steps: *i)* Compute the asymptotic behavior of the matrix $\mathbf{D}^T\mathbf{D}$ in (17), *ii)* determine the asymptotic behavior of the estimator $\hat{\eta}$ in (17), and *iii)* calculate the asymptotic behavior of the parameters $\hat{\vartheta}$ from $\hat{\eta}$. In order to simplify the analysis, we can use the fact, already noted in [2], that the ellipse fitting algorithm is invariant with respect to translations. In fact, if y_1 and y_2 are replaced by $y_1 + d_1$ and $y_2 + d_2$ for some constants d_1 and d_2, respectively, then the effect is equivalent to post-multiply $\mathbf{D}$ by a matrix

$$\mathbf{H} := \begin{bmatrix} 1 & 0 & 0 & 0 & 0 & 0 \\ 0 & 1 & 0 & 0 & 0 & 0 \\ 0 & 0 & 1 & 0 & 0 & 0 \\ 2d_1 & d_2 & 0 & 1 & 0 & 0 \\ 0 & d_1 & 2d_2 & 0 & 1 & 0 \\ d_1^2 & d_1d_2 & d_2^2 & d_1 & d_2 & 1 \end{bmatrix}.$$

However, it is easy to see that $\mathbf{H}^T\mathbf{C}\mathbf{H} = \mathbf{C}$. Therefore, the estimated ellipse will simply be a translated version of the original one. As a consequence of this, the bias and covariance of the estimated parameters $(\alpha_1, \alpha_2, \phi_\Delta, C_1, C_2)$ are independent of C_1 and C_2 (since these quantities correspond to location parameters). Therefore, in the subsequent analysis we will assume that $C_1 = C_2 = 0$ without loss of generality.

A. Asymptotic Behavior of $D^T D$

From (16) and the assumption of having independent measurements, we have that

$$\begin{aligned} \mathcal{D} &:= \lim_{N\to\infty} \frac{1}{N}\mathbf{D}^T\mathbf{D} \\ &= \begin{bmatrix} \bar{E}y_1^4 & \bar{E}y_1^3y_2 & \bar{E}y_1^2y_2^2 & \bar{E}y_1^3 & \bar{E}y_1^2y_2 & \bar{E}y_1^2 \\ \bar{E}y_1^3y_2 & \bar{E}y_1^2y_2^2 & \bar{E}y_1y_2^3 & \bar{E}y_1^2y_2 & \bar{E}y_1y_2^2 & \bar{E}y_1y_2 \\ \bar{E}y_1^2y_2^2 & \bar{E}y_1y_2^3 & \bar{E}y_2^4 & \bar{E}y_1y_2^2 & \bar{E}y_2^3 & \bar{E}y_2^2 \\ \bar{E}y_1^3 & \bar{E}y_1^2y_2 & \bar{E}y_1y_2^2 & \bar{E}y_1^2 & \bar{E}y_1y_2 & \bar{E}y_1 \\ \bar{E}y_1^2y_2 & \bar{E}y_1y_2^2 & \bar{E}y_2^3 & \bar{E}y_1y_2 & \bar{E}y_2^2 & \bar{E}y_2 \\ \bar{E}y_1^2 & \bar{E}y_1y_2 & \bar{E}y_2^2 & \bar{E}y_1 & \bar{E}y_2 & 1 \end{bmatrix} \end{aligned}$$

where $\bar{E}f := \lim_{N\to\infty} N^{-1}\sum_{n=1}^{N} E\{f(n)\}$. Here we have:

$$\begin{aligned}
\bar{E}y_1 &= \bar{E}y_2 = 0\\
\bar{E}y_1^2 &= \frac{\alpha_1^2}{2} + \sigma_1^2\\
\bar{E}y_2^2 &= \frac{\alpha_2^2}{2} + \sigma_2^2\\
\bar{E}y_1y_2 &= \frac{\alpha_1\alpha_2\cos(\phi_\Delta)}{2}\\
\bar{E}y_1^3 &= \bar{E}y_2^3 = \bar{E}y_1^2y_2 = \bar{E}y_1y_2^2 = 0\\
\bar{E}y_1^4 &= \frac{3}{8}\alpha_1^4 + 3\sigma_1^4 + 3\sigma_1^2\alpha_1^2\\
\bar{E}y_2^4 &= \frac{3}{8}\alpha_2^4 + 3\sigma_2^4 + 3\sigma_2^2\alpha_2^2\\
\bar{E}y_1^3y_2 &= \frac{\alpha_1^3\alpha_2}{8}\cos(\phi_\Delta)\\
\bar{E}y_2^3y_1 &= \frac{\alpha_1\alpha_2^3}{8}\cos(\phi_\Delta)\\
\bar{E}y_1^2y_2^2 &= \frac{\alpha_1^2\alpha_2^2}{4}\left[1+\frac{1}{2}\cos(2\phi_\Delta)\right] + \frac{\alpha_2^2}{2}\sigma_1^2 + \frac{\alpha_1^2}{2}\sigma_2^2 + \sigma_1^2\sigma_2^2.
\end{aligned}$$

Notice that most of these terms depend on σ_1^2 or σ_2^2, so it can be expected that the ellipse fitting estimator will be asymptotically biased. In fact,

$$\text{bias}\left\{\lim_{N\to\infty}\frac{1}{N}\mathbf{D}^T\mathbf{D}\right\} = \begin{bmatrix} 3\sigma_1^4+3\sigma_1^2\alpha_1^2 & 0 & \beta & 0 & 0 & \sigma_1^2\\ 0 & \beta & 0 & 0 & 0 & 0\\ \beta & 0 & 3\sigma_2^4+3\sigma_2^2\alpha_2^2 & 0 & 0 & \sigma_2^2\\ 0 & 0 & 0 & \sigma_1^2 & 0 & 0\\ 0 & 0 & 0 & 0 & \sigma_2^2 & 0\\ \sigma_1^2 & 0 & \sigma_2^2 & 0 & 0 & 0 \end{bmatrix}$$

where

$$\beta := \frac{\alpha_2^2}{2}\sigma_1^2 + \frac{\alpha_1^2}{2}\sigma_2^2 + \sigma_1^2\sigma_2^2$$

and bias $\{X\} := E\{X\} - X|_{\sigma_1=\sigma_2=0}$. The asymptotic covariance of $\mathbf{D}^T\mathbf{D}$, which is $\lim_{N\to\infty} N^{-1}\text{cov}(\text{vec}(\mathbf{D}^T\mathbf{D}))$, is a 36×36 matrix, composed of elements of the form

$$\begin{aligned}
&\lim_{N\to\infty} N[E\{(\bar{E}_N y_1^i y_2^j)(\bar{E}_N y_1^k y_2^l)\} - (E\{y_1^i y_2^j\})(E\{y_1^k y_2^l\})]\\
&= \lim_{N\to\infty}\frac{1}{N}\sum_{n=1}^{N}[E\{y_1^{i+k}(n)\}E\{y_2^{j+l}(n)\} -\\
&\qquad E\{y_1^i(n)\}E\{y_2^j(n)\}E\{y_1^k(n)\}E\{y_2^l(n)\}] \qquad (18)
\end{aligned}$$

where $i,j,k,l \in \{0,1,2,3,4\}$ and $\bar{E}_N$ is the average operator, i.e. $\bar{E}_N f := N^{-1}\sum_{n=1}^{N} f(n)$, and vec$(\cdot)$ vectorizes the matrix within the parentheses [32]. Therefore, we need to compute $E\{y_1^i(n)\}$ and $E\{y_2^i(n)\}$ for $i = 0,\ldots,8$. Now,

$$\begin{aligned}
E\{y_1^i(n)\} &= \sum_{k=0}^{i}\binom{i}{k}[\alpha_1\cos(\omega_0 n)]^{i-k}E\{v_1^k(n)\}\\
E\{y_2^i(n)\} &= \sum_{k=0}^{i}\binom{i}{k}[\alpha_2\cos(\omega_0 n+\phi_\Delta)]^{i-k}E\{v_2^k(n)\}
\end{aligned}$$

where

$$E\{v_i^k(n)\} = \begin{cases} 0, & k \text{ odd}\\ 1\cdot 3\cdots(k-1)\sigma_i^2, & k \text{ even}\end{cases}; \quad i = 1,2 \qquad (19)$$

Therefore, using Weyl's equidistribution theorem [33, Chapter 3] (assuming that ω_0 is an irrational multiple of 2π), (18) can be computed as

$$\begin{aligned}
&\lim_{N\to\infty} N[E\{(\bar{E}_N y_1^i y_2^j)(\bar{E}_N y_1^k y_2^l)\} - (E\{y_1^i y_2^j\})(E\{y_1^k y_2^l\})]\\
&= \frac{1}{2\pi}\sum_{p=0}^{i+k}\sum_{q=0}^{j+l}\binom{i+k}{p}\binom{j+l}{q}\\
&\quad\cdot\int_{-\pi}^{\pi}[\alpha_1\cos(x)]^{i+k-p}[\alpha_2\cos(x+\phi_\Delta)]^{j+l-q}dx\\
&\quad\cdot E\{v_1^p\}E\{v_2^q\} \qquad (20)\\
&-\frac{1}{2\pi}\sum_{p=0}^{i}\sum_{q=0}^{k}\sum_{r=0}^{j}\sum_{s=0}^{l}\binom{i}{p}\binom{k}{q}\binom{j}{r}\binom{l}{s}\\
&\quad\cdot\int_{-\pi}^{\pi}[\alpha_1\cos(x)]^{i+k-p-q}[\alpha_2\cos(x+\phi_\Delta)]^{j+l-r-s}dx\\
&\quad\cdot E\{v_1^p\}E\{v_1^q\}E\{v_2^r\}E\{v_2^s\}.
\end{aligned}$$

Therefore, the elements of $\lim_{N\to\infty} N^{-1}\text{cov}(\text{vec}(\mathbf{D}^T\mathbf{D}))$ can be computed from (20) and (19). We will not show the resulting covariance matrix, because of obvious space limitations.

B. Asymptotic Behavior of $\hat{\eta}$

Notice that $\hat{\eta}$, as defined in (17), satisfies the Lagrangian conditions of a local minimum:

$$\begin{aligned}
(\mathbf{D}^T\mathbf{D} - \lambda\,\mathbf{C})\,\hat{\eta} &= 0\\
\hat{\eta}^T\,\mathbf{C}\,\hat{\eta} - 1 &= 0
\end{aligned}$$

where $\lambda\in\mathbb{R}$ is a Lagrange multiplier. We can rewrite these equations in the vectorized form

$$\begin{aligned}
(\hat{\eta}^T\otimes\mathbf{I})\,(\text{vec}\{\mathbf{D}^T\mathbf{D}\} - \lambda\,\text{vec}\{\mathbf{C}\}) &= 0\\
\hat{\eta}^T\,\mathbf{C}\,\hat{\eta} - 1 &= 0 \qquad (21)
\end{aligned}$$

where $\mathbf{I}$ is the identity matrix of proper size, and $\otimes$ denotes the Kronecker product [32]. In order to study how small perturbations of vec$\{\mathbf{D}^T\mathbf{D}\}$ translate into small perturbations of $\hat{\eta}$, we can consider (21) as a function $F:\mathbb{R}^{43}\to\mathbb{R}^7$ which maps (vec$\{\mathbf{D}^T\mathbf{D}\}$, λ, $\hat{\eta}$) to the null vector. In fact,

$$F(\text{vec}\{\mathbf{D}^T\mathbf{D}\},\,\lambda,\,\hat{\eta}) = \begin{bmatrix}(\hat{\eta}^T\otimes I)(\text{vec}\{\mathbf{D}^T\mathbf{D}\} - \lambda\text{vec}\{\mathbf{C}\})\\ \hat{\eta}^T\,\mathbf{C}\,\hat{\eta} - 1\end{bmatrix}.$$

This map is continuously differentiable, with derivative

$$\frac{\partial F}{\partial[\text{vec}^T\{\mathbf{D}^T\mathbf{D}\}\;\;\lambda\;\;\hat{\eta}]} = \begin{bmatrix}\hat{\eta}^T\otimes\mathbf{I} & -\mathbf{C}\hat{\eta} & \mathbf{D}^T\mathbf{D}-\lambda\,\mathbf{C}\\ 0 & 0 & \hat{\eta}^T\,\mathbf{C}\end{bmatrix}.$$

By the implicit function theorem [34] and inversion formulae for partitioned matrices, we have the result presented in (23) (on the next page). Therefore, the asymptotic bias in $\hat{\eta}$, for small variances σ_1^2 and σ_2^2, is given by

$$\begin{aligned}
&\text{bias}(\hat{\eta}) \simeq\\
&\{(\mathbf{D}^T\mathbf{D}-\lambda\,\mathbf{C})^{-1}\mathbf{C}\eta[\eta^T\mathbf{C}(\mathbf{D}^T\mathbf{D}-\lambda\,\mathbf{C})^{-1}\mathbf{C}\eta]^{-1}\eta^T\mathbf{C} - \mathbf{I}\}\\
&\cdot(\mathbf{D}^T\mathbf{D}-\lambda\,\mathbf{C})^{-1}(\eta^T\otimes\mathbf{I})\text{bias}[\text{vec}(\mathbf{D}^T\mathbf{D})] \qquad (22)
\end{aligned}$$

$$\left[\begin{array}{c}\dfrac{\partial\lambda}{\partial \mathrm{vec}^T\{\mathbf{D}^T\mathbf{D}\}}\\ \dfrac{\partial\hat{\eta}}{\partial \mathrm{vec}^T\{\mathbf{D}^T\mathbf{D}\}}\end{array}\right]\Bigg|_{\hat{\eta}=\eta} = \left[\begin{array}{c}[\eta^T\mathbf{C}(\mathbf{D}^T\mathbf{D}-\lambda\,\mathbf{C})^{-1}\mathbf{C}\eta]^{-1}\eta^T\mathbf{C}(\mathbf{D}^T\mathbf{D}-\lambda\,\mathbf{C})^{-1}(\eta^T\otimes\mathbf{I})\\ \{(\mathbf{D}^T\mathbf{D}-\lambda\,\mathbf{C})^{-1}\mathbf{C}\eta[\eta^T\mathbf{C}(\mathbf{D}^T\mathbf{D}-\lambda\,\mathbf{C})^{-1}\mathbf{C}\eta]^{-1}\eta^T\mathbf{C}-I\}(\mathbf{D}^T\mathbf{D}-\lambda\,\mathbf{C})^{-1}(\eta^T\otimes\mathbf{I})\end{array}\right] \quad (23)$$

where $\simeq$ denotes an equality where only the dominant terms have been retained.

By the Delta method [35], the asymptotic covariance of $\hat{\eta}$ is given by

$$\begin{aligned}&\mathrm{cov}(\hat{\eta}) \simeq\\ &\{(\mathbf{D}^T\mathbf{D}-\lambda\,\mathbf{C})^{-1}\mathbf{C}\eta[\eta^T\mathbf{C}(\mathbf{D}^T\mathbf{D}-\lambda\,\mathbf{C})^{-1}\mathbf{C}\eta]^{-1}\eta^T\mathbf{C}-\mathbf{I}\}\cdot\\ &(\mathbf{D}^T\mathbf{D}-\lambda\,\mathbf{C})^{-1}(\eta^T\otimes\mathbf{I})\mathrm{cov}[\mathrm{vec}(\mathbf{D}^T\mathbf{D})](\eta\otimes\mathbf{I})(\mathbf{D}^T\mathbf{D}-\lambda\,\mathbf{C})^{-1}\\ &\cdot\{\mathbf{C}\eta[\eta^T\mathbf{C}(\mathbf{D}^T\mathbf{D}-\lambda\,\mathbf{C})^{-1}\mathbf{C}\eta]^{-1}\eta^T\mathbf{C}(\mathbf{D}^T\mathbf{D}-\lambda\,\mathbf{C})^{-1}-\mathbf{I}\}.\end{aligned}$$

Now, assuming that $\mathcal{D}:=\lim_{N\to\infty}N^{-1}\mathbf{D}^T\mathbf{D}$ is nonsingular, we obtain (for any fixed λ) that

$$\begin{aligned}\lim_{N\to\infty}N\mathrm{cov}(\hat{\eta}) = \{\mathcal{D}^{-1}\mathbf{C}\eta[\eta^T\mathbf{C}\mathcal{D}^{-1}\mathbf{C}\eta]^{-1}\eta^T\mathbf{C}-\mathbf{I}\}\mathcal{D}^{-1}\cdot\\ (\eta^T\otimes\mathbf{I})\left\{\lim_{N\to\infty}N^{-1}\mathrm{cov}[\mathrm{vec}(\mathbf{D}^T\mathbf{D})]\right\}(\eta\otimes\mathbf{I})\\ \cdot\mathcal{D}^{-1}\{\mathbf{C}\eta[\eta^T\mathbf{C}\mathcal{D}^{-1}\mathbf{C}\eta]^{-1}\eta^T\mathbf{C}\mathcal{D}^{-1}-\mathbf{I}\}. \quad (24)\end{aligned}$$

It is possible to reduce the size of these expressions (and thus the computational burden on their symbolic simplification) by introducing a small perturbation and using the matrix inversion lemma [36]:

$$\begin{aligned}&\{\mathcal{D}^{-1}\mathbf{C}\eta[\eta^T\mathbf{C}\mathcal{D}^{-1}\mathbf{C}\eta]^{-1}\eta^T\mathbf{C}-\mathbf{I}\}\mathcal{D}^{-1}\\ &\qquad=-\lim_{\varepsilon\to0}(\mathcal{D}+\varepsilon^{-1}\mathbf{C}\eta\eta^T\mathbf{C})^{-1}.\end{aligned}$$

Therefore, (24) can be written as

$$\begin{aligned}\lim_{N\to\infty}N\mathrm{cov}(\hat{\eta}) = \left[\lim_{\varepsilon\to0}(\mathcal{D}+\varepsilon^{-1}\mathbf{C}\eta\eta^T\mathbf{C})^{-1}\right](\eta^T\otimes\mathbf{I})\\ \cdot\left\{\lim_{N\to\infty}N^{-1}\mathrm{cov}[\mathrm{vec}(\mathbf{D}^T\mathbf{D})]\right\}\cdot \quad (25)\\ (\eta\otimes\mathbf{I})\left[\lim_{\varepsilon\to0}(\mathcal{D}+\varepsilon^{-1}\mathbf{C}\eta\eta^T\mathbf{C})^{-1}\right]\end{aligned}$$

and, as for (22),

$$\begin{aligned}\mathrm{bias}(\hat{\eta}) \simeq -\left[\lim_{\varepsilon\to0}(\mathcal{D}+\varepsilon^{-1}\mathbf{C}\eta\eta^T\mathbf{C})^{-1}\right]\\ \cdot(\eta^T\otimes\mathbf{I})\mathrm{bias}\left[\lim_{N\to\infty}N^{-1}\mathrm{vec}(\mathbf{D}^T\mathbf{D})\right].\end{aligned}$$

C. Asymptotic Behavior of $\hat{\vartheta}$

Let ϑ be given by (8). Using the Delta method, the relations between the elements in η and ϑ, and (25), we have that

$$\mathrm{cov}(\vartheta) \simeq \frac{\partial\vartheta}{\partial\eta^T}\mathrm{cov}(\hat{\eta})\frac{\partial\vartheta^T}{\partial\eta}$$

where the gradients must be evaluated at the true value of η, and

$$\mathrm{bias}(\vartheta) \simeq \frac{\partial\vartheta}{\partial\eta^T}\mathrm{bias}(\hat{\eta})$$

where

$$\frac{\partial\vartheta}{\partial\eta^T} = \left[\begin{array}{cccccc}0&0&\sqrt{\frac{|f|}{c}}&0&0&-\sqrt{\frac{c}{|f|}}\\ \sqrt{\frac{|f|}{a}}&0&0&0&0&-\sqrt{\frac{a}{|f|}}\\ -\frac{2b}{a}&1&-\frac{b}{2c}&0&0&0\\ 0&0&0&-2c&b&0\\ 0&0&0&b&-2a&0\end{array}\right]_{\hat{\eta}=\eta}.$$

This expression has to be evaluated in terms of $(\alpha_1,\alpha_2,\phi_\Delta)$ by using (15).

D. High SNR Approximation

The analysis carried out in the previous subsections gives a full description of the asymptotic covariance of the ellipse fitting algorithm. However, the size of the resulting expressions is too long to provide some intuition about the qualitative behavior of the method. Therefore, in order to obtain such an intuition, we will consider a special case based on the following simplifying assumptions:

1) $\sigma_1^2=\sigma_2^2=\sigma^2$.
2) $\phi_\Delta=\pi/2$.
3) σ is *small*.

Under these conditions, the asymptotic covariance of the parameters $(\alpha_1,\alpha_2,\phi_\Delta,C_1,C_2)$ is:

$$\begin{aligned}&\mathrm{cov}(\vartheta) \simeq\\ &\left[\begin{array}{ccccc}\frac{\sigma^2(\alpha_1^2+5\alpha_2^2)}{2N\alpha_2^2}&-\frac{\sigma^2(\alpha_1^2+\alpha_2^2)}{2N\alpha_1\alpha_2}&0&0&0\\ -\frac{\sigma^2(\alpha_1^2+\alpha_2^2)}{2N\alpha_1\alpha_2}&\frac{\sigma^2(5\alpha_1^2+\alpha_2^2)}{2N\alpha_1^2}&0&0&0\\ 0&0&2\frac{\mathrm{SNR}_1+\mathrm{SNR}_2}{N\,\mathrm{SNR}_1\,\mathrm{SNR}_2}&0&0\\ 0&0&0&\frac{\sigma^2(\alpha_1^2+3\alpha_2^2)}{2N\alpha_2^2}&0\\ 0&0&0&0&\frac{\sigma^2(3\alpha_1^2+\alpha_2^2)}{2N\alpha_1^2}\end{array}\right]\end{aligned}$$

where the SNR was defined in (11). As it can be noted by comparing this matrix with Table I, the variances of α_1 and α_2 are within $5/4$ and $3/2$ times their Cramér-Rao bound, the variance of ϕ_Δ is twice its CRB, and the variances of C_1 and C_2 are within $3/2$ and 2 times their CRB. This implies that the ellipse fitting algorithm is *not* statistically efficient.

Under the same assumptions, the bias of the parameters $(\alpha_1,\alpha_2,\phi_\Delta,C_1,C_2)$ is:

$$\mathrm{bias}(\vartheta) \simeq \left[\begin{array}{c}\frac{5\alpha_2^2-3\alpha_1^2}{2\alpha_1\alpha_2^2}\sigma^2\\ \frac{5\alpha_1^2-3\alpha_2^2}{2\alpha_2\alpha_1^2}\sigma^2\\ 0\\ 0\\ 0\end{array}\right].$$

E. Results for IQ parameters

In order to determine the variance and bias of the IQ parameter estimates $\hat{G}$, $\hat{Q}$ and $\hat{L}$ (obtained by simply replacing the parameters $(\alpha_1, \alpha_2, \phi_\Delta, C_1, C_2)$ by their estimates in the definitions of such quantities), we can use the Delta method and Taylor series expansions. This gives (using the notation of Table I):

$$\begin{aligned}
\text{var}(\hat{G}) &\simeq \frac{2G^2}{N}\left[\frac{1}{\text{SNR}_1}+\frac{1}{\text{SNR}_2}\right] \\
\text{var}(\hat{Q}) &\simeq 2\frac{\text{SNR}_1+\text{SNR}_2}{N\,\text{SNR}_1\,\text{SNR}_2} \\
\text{var}(\hat{L}) &\simeq \frac{2L(2+L)}{N\text{SNR}}
\end{aligned}$$

and

$$\begin{aligned}
\text{bias}(\hat{G}) &\simeq \frac{4(\alpha_1^2-\alpha_2^2)\sigma^2}{\alpha_1^3\alpha_2} \\
\text{bias}(\hat{Q}) &\simeq 0 \\
\text{bias}(\hat{L}) &\simeq -\frac{L}{\text{SNR}}.
\end{aligned}$$

Note that for the statistics of $\hat{L}$ we have assumed $\alpha_1 = \alpha_2$ (but *not* $C_1, C_2 = 0$) in order to obtain expressions comparable to those of Table I.

The bias of $\hat{G}$ is positive if and only if $\alpha_1 > \alpha_2$, hence $\hat{G}$ is biased towards 1. This agrees with [2], where it is observed that the ellipse fitting algorithm possesses a *low eccentricity bias*, i.e., it tends to give ellipses which are closer to being a circle than a line.

V. Simulation example

In order to verify the theoretical results presented in the previous section, we consider a scenario presented in [20], where the performance of a nonlinear least squares method was analyzed. The setup is given by $G = 1.0$ dB, $Q = 1.0^\circ$ and $L = -40.0$ dB. The noise affecting the measurements is white and Gaussian, with $\text{SNR}_1 = \text{SNR}_2 = 74.0$ dB, which corresponds to the signal-to-noise ratio due to the use of an analog-to-digital converter of 12 bits. $N = 128$ samples are taken, and the angular frequency of the sinusoids is $\omega_0 = 0.15$ rad/s. The result of running 100000 Monte Carlo simulations is presented in Figure 1, which shows the empirical histogram of the estimates obtained using the ellipse fitting algorithm, in conjunction with their theoretical (asymptotic) distributions, and the distribution of a normal asymptotically efficient estimator (such as the one presented in [20]).

Figure 1 shows the excellent agreement between the simulation and theoretical results, even for a small sample size of 128. It is also interesting to note that the theoretical bias of the IQ parameters under this scenario is quite negligible: $|\text{bias}\{\hat{G}\}| \simeq -77.9$ dB and $|\text{bias}\{\hat{L}\}| \simeq -114.0$ dB.

VI. Experiments

In this section the ellipse based IQ imbalance estimation scheme derived in Section III is applied on measurements obtained from five samples of the universal software radio peripheral (USRP2), all equipped with a XCVR2450 daughterboards (www.ettus.com). These daughterboards are designed around the Maxim MAX2829 BiCMOS transceiver chip (www.maxim-ic.com/datasheet/index.mvp/id/4532/t/al) which is aimed at smart-antenna/MIMO applications in the 2.4/5GHz ISM-bands using IEEE802.11b related standards. Here we investigate the scattering of the IQ parameters, ϑ, using batches of only $N = 128$ samples as compared to using $N = 30000$ samples. We further investigate whether the IQ parameters, ϑ, vary with the input signal frequency ω_0, see (4). The variation with frequency ω_0 would indicate if a frequency dependent compensation scheme is needed [37]. We further investigate the variation with respect to carrier frequency, time and across hardware units.

In a commercial implementation of the IQ parameter estimation scheme one may either perform the measurements during production tests or using on-line measurements when the node is idle. A node with two antennas could transmit the calibration signal from one of its transceivers to the other, A third possibility is to consider the IQ parameters as part of the transmission channel and estimate them in every burst [38]. Here we investigate the usefulness of the first two of these approaches by studying the variation of the IQ parameters, ϑ, with base-band frequency, carrier frequency, time, and between individual XCVR2450 daughterboards. Obviously, if there are no variations in time or across units a single calibration table would suffice, and neither factory- nor online-calibration would be required. However, the results show significant variation in all dimensions except time. This indicates that a factory calibration would indeed be sufficient. However, the variation with base-band and carrier frequency shows that a table of calibration values would be needed.

A. Measurement setup and pre-processing

The receiving end of one XCVR2450 is connected to the transmitting end of another XCVR2450 by means of a cable and 25dB of extra attenuators. The signal from the transmitter XCVR2450 is generated in Matlab using a base-band sample-frequency of 25MHz. The signal is then transferred from the host PC to the USRP2 which up-samples and D/A converts it at 100MHz. The D/A converters (IQ) of the USRP2 are connected to the transmitter XCVR2450. Conversely, on the receiver side the XCVR2450 are connected to A/D converters which sample at 100MHz. The samples are then decimated to 25MHz and sent to the hosting PC by the USRP2. The USRP2 and the XCV2450s are both sample and carrier-frequency synchronized from the same 10MHz reference. The sampling is triggered using the "time-stamp" functionality of the USRP2 UHD driver software (www.ettus.com). The driver has been slightly modified to remove any digital up- or down-conversion.

Since the transmitter as well as the receiver have DC offset and IQ imbalance, it is normally difficult to separate the effects of the transmitter and receiver. However, here we add an offset of 500kHz between the transmitter and receiver carrier (tuning) frequencies. Thus, when we generate a base-band cisoid of frequency f_{TX} at the transmitter, it is received at frequency

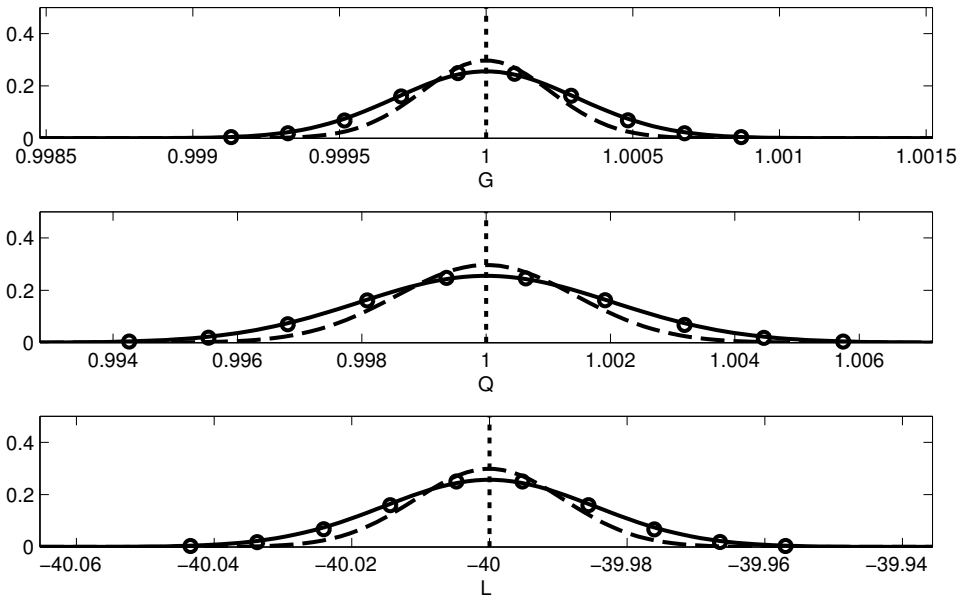

Fig. 1: Histograms of the estimates of G, Q and L, obtained using the ellipse fitting algorithm (shown as circles). The solid lines correspond to the asymptotic distribution predicted by the the theory of Section IV. The dashed lines represent the asymptotic distribution of an efficient estimator. The true values are shown with a vertical dotted line.

$f_{\text{TX}} + 500$ kHz. The mirror signal of the transmitter is located at $-f_{\text{TX}} + 500$ kHz while the receiver mirror signal is located at $-f_{\text{TX}} + 500$ kHz. The DC offset of the transmitter will turn up as a cisoid of 500 kHz while the DC offset of the receiver is located at 0 Hz.

In order to test several base-band frequencies, the base-band signal is chosen as a sequence of cisoids with frequencies between -10.5 MHz to 9.5 MHz with a step size of 0.5 MHz. Each cisoid contains 30000 useful samples plus guard time for transients. When analyzing the IQ parameters of the receiver the mirror and DC component of the transmitter are first filtered. When analyzing the IQ parameters of the transmitter, the signal is first frequency translated in based-band by multiplying the received data by a cisoid with -500 kHz frequency, followed by filtering to remove the receiver mirror frequency and DC offset. After performing these pre-processing steps, the real and imaginary part of the estimations are used as y_1 and y_2 respectively.

B. Small-sample performance

In Figure 2, histograms of the G,Q and L estimates obtained from the receiver of XCVR2450 number one are shown[1]. The results are obtained using a batch of $N = 128$ samples. Also indicated, in red, is the estimate obtained using all samples in a single batch. The results show that the small batch estimation deviates up to 0.03 dB in gain imbalance and up to 0.3 degrees in phase, at the receiver. We have found that the estimation variance decreases in inverse proportion to the number of samples, as predicted by the theoretical analysis. The number of samples needs to be selected in order to obtain the desired performance.

[1]We have five copies XCVR2450 which we have numbered arbitrarily.

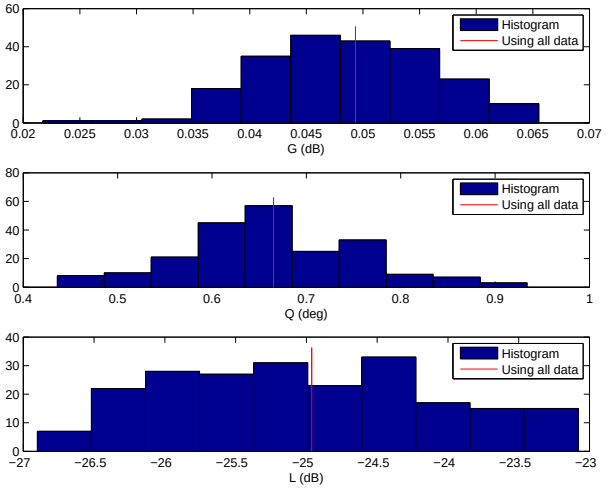

Fig. 2: Estimates obtained using $N = 128$ samples (histogram), or all samples (red line). Receiver of XCVR2450 #1, carrier frequency 4900 MHz, and base-band frequency 2 MHz.

The phase and gain imbalance at the transmitters have been found to be consistently much smaller than at the receiver. In the following we will therefore concentrate on the receiver imbalance.

The DC offset is of less importance than the phase skew and gain imbalance because OFDM modulations generally does not use the subcarrier at the DC component.

The numbers presented here are well in-line with those stated in the data-sheet of the circuit.

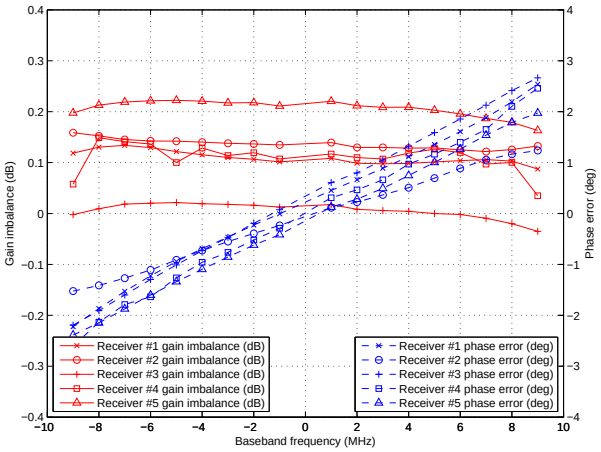

Fig. 3: Estimates of the gain skew and phase imbalance as a function of the base-band frequency ω_0, the carrier frequency is 4900 MHz.

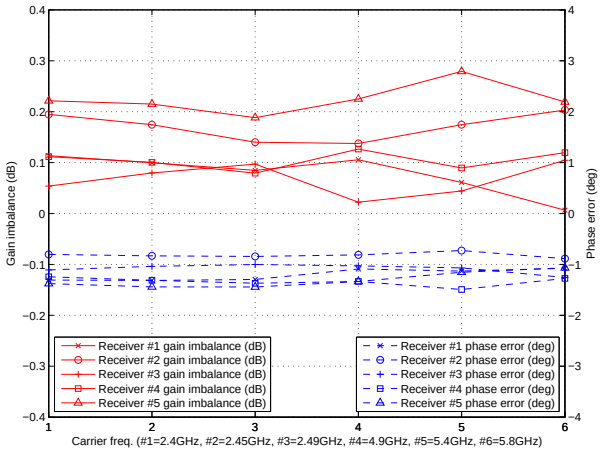

Fig. 4: Estimates of the gain imbalance and phase imbalance as a function of the carrier frequency for a fixed base-band frequency of -5 MHz.

C. Variation with base-band frequency ω_0

Figure 3 shows the variation of the gain imbalance and phase-skew for the receiving end of all our five XCVR2450 units as a function of the base-band frequency ω_0. The results show that the phase skew is clearly varying with ω_0 while the gain imbalance is rather constant. On the other hand, the variation in gain imbalance is substantial among units. These results show that calibration and compensation methods need to consider variations with respect to the base-band frequency ω_0 and to use individual compensations for different hardware units.

D. Variation with carrier frequency

Figure 4 shows the variation of the gain imbalance and phase-imbalance of the receiving end of all our five XCVR2450 units as a function of the the carrier frequency. The base-band frequency is fixed at -5 MHz. The gain imbalance is varying so much that a carrier frequency dependent compensation is needed.

E. Variation with time

Figure 5 shows the variation of the gain imbalance and phase-imbalance of the receiving end of two XCVR2450 during an eighteen hour run. One measurement was done every minute. The base-band frequency is fixed at -5 MHz. It should be noted that there was actually a gap of 66 hours between measurements #540 and #541. The two receivers were measured almost simultaneously. At about 6 hours the measurement sequence of both receivers show a transient. Since both measurements were conducted simultaneously this transient may have a common source. The most likely cause is a rising temperature. Both receivers were located nearby a window and direct sunlight enters this window at this time. However, the magnitude of the transient is negligible (as it can be seen from the scale of the y-axis). Therefore, our measurements indicate that a calibration in production should be enough.

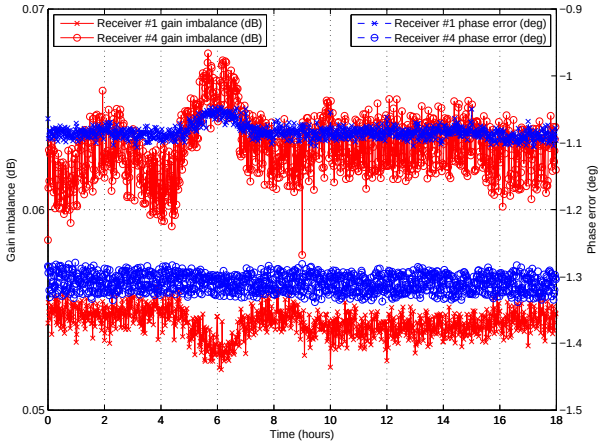

Fig. 5: Estimates of the gain imbalance and phase imbalance as a function of time $\omega_0/2\pi = -5$ MHz. There is a gap of 66 hours between measurement #540 and #541. The two receivers were measured simultaneously.

VII. Conclusions

In this paper we have introduced and analyzed a method for the estimation of the IQ imbalance parameters in transceivers. The method, based on an ellipse fitting technique, is simple, fast, non-iterative and relatively accurate. Our analysis has shown that the proposed method has low bias and a variance within a factor of 2 of the CRB for the G and Q parameters, and a factor of 4 for the L parameter. These results have been verified by a numerical simulation example.

We have also applied the derived method on measurements of a contemporary BiCMOS transceiver called MAXIM 2829. From these measurements we found that the IQ imbalance varied with base-band frequency, carrier frequency, and across the five different hardware units, while the variation with time was small. In our measurements the phase skew varies up to five degrees with the base-band frequency, while the amplitude imbalance varies between 0-0.3dB over carrier frequencies

and across hardware units. The time variation however is only 0.004dB in amplitude and 0.06degrees in phase. This indicates that the units could either be calibrated on-line when there is no transmission (in a two antenna MIMO system one antenna could transmit a calibration signal to the other). Another alternative would be to calibrate during production in which a case a table with different carrier and base-band frequencies would be needed. However, there is no need to estimate the parameters on every burst.

REFERENCES

[1] M. Vidmar. "K-band quadrature mixers with plastic-packaged diodes," *Microwave Journal*, 22–40, January 2000.

[2] A. Fitzgibbon, M. Pilu and R. B. Fisher, "Direct least square fitting of ellipses," *IEEE Transactions on Pattern Analysis and Machine Intelligence*, Vol. 21, Issue 5, pp. 476-480, 1999.

[3] N. Ray, S.T. Acton and K. Ley, "Tracking leukocytes in vivo with shape and size constrained active contours," *IEEE Transactions on Medical Imaging*, Vol. 21, Issue 10, October 2002, pp. 1222-1235.

[4] V. Pratt, "Direct least-squares fitting of algebraic surfaces," *Computer Graphics*, vol. 21, no. 4, 1987, 145–152.

[5] W. Gander, G. H. Golub and R. Strebel, "Least-squares fitting of circles and ellipses," *BIT*, vol. 34, 1994, 558–578.

[6] B. Matei and P. Meer, "Reduction of bias in maximum likelihood ellipse fitting," in *Proceedings of the 15th International Conference on Pattern Recognition (ICPR-2000)*, Barcelona, Spain, September 2000, 794–798 (vol. 3).

[7] W. Chojnacki, M. J. Brooks, A. van den Hengel and D. Gawley, "On the fitting of surfaces to data with covariances," *IEEE Transactions on Pattern Analysis and Machine Intelligence*, vol. 22, no. 11, 2000, 1294–1303.

[8] K. Kanatani, "Ellipse fitting with hyperaccuracy," in *Proceedings of the 9th European Conference on Computer Vision (ECCV 2006)*, Graz, Austria, May 2006, 484–485 (vol. 1).

[9] J.A. Lissajous, "Memoire sur l'etude optique des mouvements vibratoires," *Annales de Chimie et de Physique*, Paris, Victor Masson Librairie, vol. LI, October 1857, pp. 147-232.

[10] P. Händel and A. Høst-Madsen, "Estimation of velocity and size of particles from two channel laser anemometry measurements," *Measurement*, vol. 21, no. 3, 113-123, July 1997.

[11] A. Høst-Madsen and K. Andersen, "Lower bounds for estimation of frequency and phase of Doppler signals," *Measurement Science and Technology*, vol. 6, 637-652, 1995.

[12] P.M. Ramos, F.M. Janerio and T. Radil, "Comparison of impedance measurements in a DSP using ellipse-fit and seven-parameter sine-fit algorithms," *Measurement*, Vol. 42, Issue 9, November 2009, Pages 1370-1379.

[13] P.M. Ramos, F.M. Janeiro, M. Tlemcani, A.C. Serra, "Recent developments on impedance measurements with DSP-based ellipse-fitting algorithms," *IEEE Transactions on Instrumentation and Measurement*, Vol. 58, Issue 5, May 2009, pp. 1680 - 1689.

[14] P.M. Ramos, M. Fonseca da Silva and A. Cruz Serra, "Low frequency impedance measurement using sine-fitting," *Measurement*, vol. 35, no. 1, 89-96, January 2004.

[15] T. Radil, P.M. Ramos and A. Cruz Serra, "Impedance measurement with sine-fitting algorithms implemented in a DSP portable device," *IEEE Transactions on Instrumentation and Measurements*, vol. 57, no. 1, 197-204, January 2008.

[16] P. Händel, "Parameter estimation employing a dual channel sinewave model under a Gaussian assumption," *IEEE Transactions on Instrumentation and Measurement*, Vol. 57, No. 8, August 2008, pp. 1661-1669, doi:10.1109/TIM.2008.923782.

[17] S.M. Kay, *Fundamentals of Statistical Signal Processing: Estimation Theory*, vol. 1. Upper Saddle River, NJ: Prentice-Hall, 1993.

[18] P.M. Ramos and A. Cruz Serra, "A new sine-fitting algorithm for accurate amplitude and phase measurements in two channel acquisitions," *Measurement*, vol. 41, no. 2, 135-143, February 2008.

[19] P. Händel, "Properties of the IEEE-STD-1057 four-parameter sine wave fit algorithm", *IEEE Transactions on Instrumentation and Measurement*, Vol. 49, No. 6, pp. 1189-1193, December, 2000.

[20] P. Händel and P. Zetterberg, "Receiver IQ imbalance: tone tests, sensitivity analysis, and the universal software radio peripheral," *IEEE Transactions on Instrumentation and Measurement*, Vol. 59, No. 3, March 2010, pp. 704-714, doi:10.1109/TIM.2009.2025989.

[21] S. Cass, "Hardware for your software radio," *IEEE Spectrum*, Vol. 43, No. 10, October 2006, pp. 51-56.

[22] J. McEllroy, J.F. Raquet, M.A. Temple, "Use of a software radio to evaluate signals of opportunity for navigation," *19th International Technical Meeting of the Satellite Division, ION GNSS*, Vol. 1, 2006, pp. 126-133.

[23] Zhi Yan, Zhangchao Ma, Hanwen Cao, Gang Li, Wenbo Wang, "Spectrum sensing, access and coexistence testbed for cognitive radio using USRP," *4th IEEE International Conference on Circuits and Systems for Communications*, 26-28 May 2008, pp. 270-274.

[24] R. Dhar, G. George, A. Malani, P. Steenkiste, "Supporting integrated MAC and PHY software development for the USRP SDR," *1st IEEE Workshop on Networking Technologies for Software Defined Radio Networks*, 25-25 September 2006, pp. 68-77.

[25] G. Zoka, "Refined I/Q: Imbalance measurements," *Microwaves and RF*, vol. 43, no. 6, pp. 72-83, 2004.

[26] T. Andersson and P. Händel, "IEEE standard 1057, Cramér-Rao bound and the parsimony principle," *IEEE Transactions on Instrumentation and Measurements*, vol. 55, no. 1, 44-53, February 2006.

[27] D. Rife and R. Boorstyn, "Single tone parameter estimation from discrete-time observations," *IEEE Transactions on Information Theory*, vol. 20, no. 5, 591-598, 1974.

[28] Y. T. Chan and S. M. Thomas, "Cramér-Rao lower bounds for estimation of a circular arc center and its radius," *Graphical Models and Image Processing*, vol. 57, no. 6, 1995, 527–532.

[29] K. Kanatani, "Cramér-Rao lower bounds for curve fitting," *Graphical Models and Image Processing*, vol. 60, no. 2, 1998, 93–99.

[30] N. Chernov and C. Lesort, "Statistical efficiency of curve fitting algorithms," *Computational Statistics & Data Analysis*, vol. 47, 2004, 713–728.

[31] M. Valkama, M. Renfors and V. Koivunen, "Advanced methods for I/Q imbalance compensation in communication receivers," *IEEE Transactions on Signal Processing*, Vol. 49, No. 10, October 2001, pp. 2335-2344.

[32] J. W. Brewer. "Kronecker Products and Matrix Calculus in System Theory," *IEEE Transactions on Circuits and Systems*, vol. 25, no. 9, 772-781, 1978.

[33] T. W. Körner. *Fourier Analysis*. Cambridge University Press, 1988.

[34] T. W. Gamelin and R. E. Greene. *Introduction to Topology, 2nd Edition*. Dover, 1999.

[35] G. Casella and R. L. Berger. *Statistical Inference, 2nd Edition*. Duxbury, 2002.

[36] W. W. Hager, "Updating the inverse of a matrix," *SIAM Review*, vol. 31, no. 2, 221–239, 1989.

[37] M. Valkama, M. Renfors, and V. Koivunen "Compensation of Frequency- Selective I/Q Imbalances in Wideband Receivers: Models and Algorithms"in Proc. Third IEEE Signal Processing Workshop Signal Processing Adv. Wireless Commun. (SPAWC01), Taoyuan, Taiwan, R.O.C., March 2001, pp. 42-45.

[38] K.Hao Lin, H.L Lin, S.M Wang, and R.C Chang. "Implementation of digital IQ imbalance compensation in OFDM WLAN receivers". IEEE Int. Symposium on Circuits and Systems, Nov 2006.